RSC Advances

PAPER

View Article Online
View Journal | View Issue



Cite this: *RSC Adv.*, 2019, **9**, 28768

# Preparation of recyclable $MoO_3$ nanosheets for visible-light driven photocatalytic reduction of Cr(VI)

Wenxian Wei,[a] Zhenxin Zhang,[a] Guoxiang You,[b] Yun Shan*[c] and Zuozheng Xu[a]

Received 22nd July 2019
Accepted 29th August 2019

DOI: 10.1039/c9ra05644k

rsc.li/rsc-advances

The exploitation of stable and earth-abundant photocatalysts with high catalytic activity remains a significant challenge for removing heavy metals from wastewater. Different from complex nanostructuring, this work focuses on a simple and feasible way to design catalysts. Herein, $MoO_3$ nanosheets were fabricated and grown vertically on the surface of a quartz tablet using a one-step chemical vapor deposition method. The morphology, construction and optical properties of the $MoO_3$ were characterized by XRD, XPS, SEM, HRTEM and UV-Vis methods, and the possible growth mechanism was also discussed. It can be found that the $MoO_3$ nanosheets exhibited significantly enhanced visible light photocatalytic reduction capacity with stable recyclability to Cr(VI). The results show that the $MoO_3$ nanosheets can be used as a cost-effective and recyclable photocatalyst for the removal of Cr(VI) from water. Our findings provide new inspiration for the design of new types of catalysts.

## 1. Introduction

Wastewater always contains heavy metals and organic compounds which endanger the environment. As is well known, chromium is widely used in many fields such as mining, chemical manufacturing, electroplating and leather making and processing, and pollution caused by chromium, mainly Cr(VI), has been ranked among the top ten worst toxic contamination issues according to a report released in 2012.[1,2] Thus, the removal of Cr(VI) in water has great significance to our environment.

Environmental friendly catalytic processes are increasingly receiving attention nowadays, and photocatalytic technology provides a method for overcoming the problems.[3] The photocatalysis is a physico-chemical process in which chemical reactions are driven using light energy and photocatalysts.[4] Semiconducting nanomaterials have been widely used as photocatalysts because they are unique in nature of the mechanical, optical, electrical, catalytic and magnetic properties.[5–8]

As a n-type semiconductor, molybdenum trioxide ($MoO_3$) can be used in catalytic, optical and electrochemical applications, and compared to other metal oxide materials, $MoO_3$ has low cost, good structural stability and less toxicity.[9–11] For example, assembled-sheets-like $MoO_3$ was synthesized with a facile heat treatment route and used as an anode for lithium ion batteries, which maintained an improved discharge capacity over 100 cycles with capacity retention of ~100%;[12] Wang *et al.* prepared ultrafine β-$MoO_3$ from industrial grade $MoO_3$ powder *via* the method of sublimation and discussed its growth mechanism;[13] Pandeeswari *et al.* fabricated nanostructured α-$MoO_3$ thin film as a highly selective TMA sensor;[14] by a solution combustion reaction, ultra-porous $MoO_3$ can be obtained with both excellent photocatalytic and electrochemical properties.[15]

Therefore, the development of $MoO_3$ nanoparticles has consequently increased in recent years.[16–20] By now, many synthesis processes of $MoO_3$ are widely investigated using electrodeposition, molten salt, hydrothermal, sol–gel methods *et al.*, and different morphologies including nanofibers, microbelts and flower-like spheres can be fabricated.[21–26]

Nowadays $MoO_3$ has been widely used as photocatalysts. As reported in ref. 27, three-dimensional $MoO_3$ nanoflowers assembled with nanosheets were fabricated by the modified hydrothermal method for degradation of RhB under visible light; Liu *et al.* fabricated hierarchical porous monoliths of $MoO_3$ nanoplates. The as-prepared $MoO_3$ exhibited strong adsorption performance and excellent photocatalytic activity as well as promising cyclic performance for photodegradation of MB;[28] $MoO_3$ microrods were synthesized using leaf extract of *Azadirachta indica* and used for the cationic dye degradation;[29] Ma *et al.* prepared $MoO_3$ nanoflake on conjugated polymer for hydrogen evolution from water solution under solar light.[30]

It is known that two-dimensional materials shows very interesting physical and chemical characteristics.[31–33] In this

[a]*Testing Center, Yangzhou University, Yangzhou, Jiangsu 225009, China*
[b]*Key Laboratory of Integrated Regulation and Resources Development on Shallow Lakes, Ministry of Education, College of Environment, Hohai University, Nanjing, Jiangsu 210098, China*
[c]*Key Laboratory of Advanced Functional Materials of Nanjing, Nanjing Xiaozhuang University, Nanjing 211171, China. E-mail: gangzhou361@163.com; Tel: +86-516-83262091*

work, $MoO_3$ nanosheets which deposited vertically on the surface of quartz tablet were fabricated by one-step chemical vapor deposition method. The morphology, construction and optical properties of $MoO_3$ were characterized by XRD, XPS, SEM, HRTEM, UV-Vis methods, respectively. The photocatalytic and recyclable performance of the as-prepared $MoO_3$ on the degradation Cr(VI) were analyzed. The fabrication process is low energy consumption, easy to operate and environmentally friendly. Meanwhile, the $MoO_3$ deposited on quartz tablet is easy to be separated from water, which avoids secondary pollution during using process. Thus, the as-prepared $MoO_3$ exhibits good application prospect for solving the pollution problems in water.

## 2. Experimental section

### 2.1 Materials

All chemicals including molybdenum disulfide ($MoS_2$) and potassium dichromate ($K_2Cr_2O_7$) are analytically pure and used as received without further purification. Deionized water was used for all procedures.

### 2.2 Preparation of $MoO_3$ nanosheets

$MoO_3$ nanosheets were prepared by chemical vapor deposition. As shown in Fig. 1, 0.2 g $MoS_2$ were placed in a combustion boat on the middle of the tube furnace, and then a piece of quartz tablet (1 × 1 cm) was placed behind the $MoS_2$ with a distance of about 15 cm, and 517 sccm argon gas was pumped for 40 min. After that, the tube furnace was vacuum pumping till $7.5 \times 10^{-2}$ Torr, and then heated to 900 °C with the heating rate of 10 °C $min^{-1}$. The reaction was kept for 20 min with Ar flow of 26 sccm and $O_2$ flow of 4 sccm. Finally the system was cooled to room temperature and the quartz tablet coated with products was taken out for further analysis.

### 2.3 Characterization

Scanning electron microscope (SEM) images were obtained using a HITACHI S-4800 microscope (Japan). High-resolution transmission electron microscopy (HRTEM) images were obtained using a FEI Tecnai G2 F30 microscope (USA). The phase purity of the product was characterized by X-ray diffraction (XRD, German Bruker AXSD8 ADVANCE X-ray diffractometer) using an X-ray diffractometer with Cu KR radiation ($\lambda = 1.5418$ Å). The ultraviolet-visible (UV-Vis) diffuse reflectance spectra were obtained on an America Varian Cary 5000 spectrophotometer. Raman spectra were measured using a Britain Renishaw inVia Raman spectrometer at room temperature.

### 2.4 Photocatalytic experiments

The degradation of $K_2Cr_2O_7$ was proceeded using the as-prepared $MoO_3$ nanosheets as photocatalysts with visible lights. Cr(VI) stock solution (10 mg $L^{-1}$) was prepared by dissolving $K_2Cr_2O_7$ in distilled water. After the a piece of $MoO_3$-coated quartz tablet was immersed in 20 mL of Cr(VI) solution, the resulting solution was magnetically stirred in the dark for 30 min at room temperature. Then the photocatalytic experiments were carried out in a GHX-2 photochemical reactor as report in ref. 34 and 35, which includes mainly four parts: light source system including a 300 W xenon lamp with a 420 nm cut-off filter and cooling attachments such as electric fan; reactor (two-layer Pyrex glass bottles of 400 mL capacity, the space between the two layers is filled with circulating water to cool the reactor); magnetic stirrer; and temperature controller. In each experiment, the distance between the xenon lamp and the reactor was set to be 5.8 cm, and the reaction temperature was 25 °C. At an interval of 10 min, 3 mL of the solution was extracted and monitored *via* UV-Vis spectrometer.

The photocatalytic efficiency of Cr(VI) could be calculated according to the following equation: % degradation = $(1 - A_t/A_0) \times 100\%$, where $A_0$ and $A_t$ are the initial absorbance and absorbance at time '$t$' of Cr(VI).[36]

Besides, as referential photocatalysts, 0.8 mg $TiO_2$ (P25) and 0.8 mg $MoS_2$ nanosheets were respectively used for degradation of Cr(VI).

## 3 Results and discussion

### 3.1 Characterizations

Fig. 2(a) displayed XRD patterns of the as-prepared $MoO_3$. Diffraction peaks of the product is in good agreement with orthorhombic α-$MoO_3$ (JCPDS card no. 05-0508) and the main peaks observed at 12.9°, 23.5°, 26.1°, 27.4° and 39.2° are corresponding to the (020), (110), (040), (021) and (060) planes. No other peaks of impurities were detected. The sample exhibits sharp peaks which ascribable to its highly crystalline nature.

Fig. 2(b) shows the typical Raman spectra of $MoO_3$ nanosheets. The Raman peaks at 819 $cm^{-1}$ and 995 $cm^{-1}$ should be induced by the symmetric and asymmetric stretching vibration modes of terminal bond Mo=O. The asymmetric stretching vibration mode of O–Mo–O was assigned at 665 $cm^{-1}$, while the

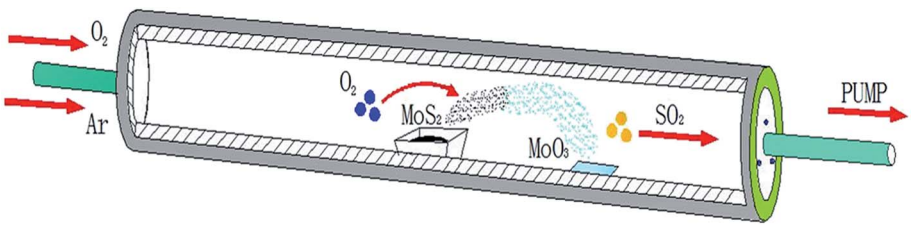


Fig. 1 The fabrication process for $MoO_3$ using CVD method.

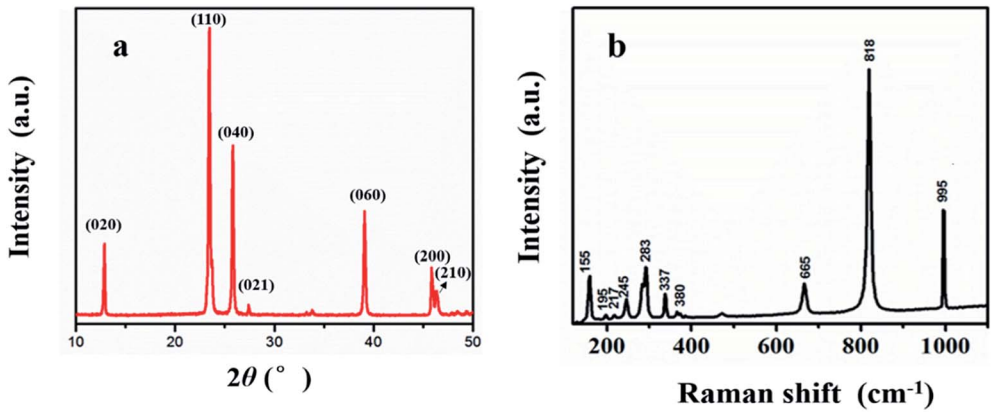


Fig. 2 (a) XRD and (b) Raman spectra of $MoO_3$.

Raman peaks at 380 $cm^{-1}$, 337 $cm^{-1}$, 283 $cm^{-1}$ and 245 $cm^{-1}$ indicated the vibrating bending modes in $MoO_3$.[11]

According to XRD and Raman analytical results, it can be found that the product is well-crystallized $MoO_3$.

XPS analysis was performed in further to confirm the presence of elements of Mo. Fig. 3(a) shows that the peaks in the spectra were assigned to Mo, O, and C. From Fig. 3(b), two peaks located at 233 eV and 236 eV can be respectively due to Mo $3d_{1/2}$ and Mo $3d_{3/2}$ signals, ensuring the $Mo^{6+}$ valence state.[28] Besides, the atom ratio of Mo and O is about 1 : 3, in further proving the formation of $MoO_3$.

The morphology of the as-prepared $MoO_3$ was characterized *via* SEM and TEM respectively and the results can be found in Fig. 4(a)–(d).

From SEM images, it can be found that $MoO_3$ nanosheets were uniformly grown vertically on the surface of the substrate,

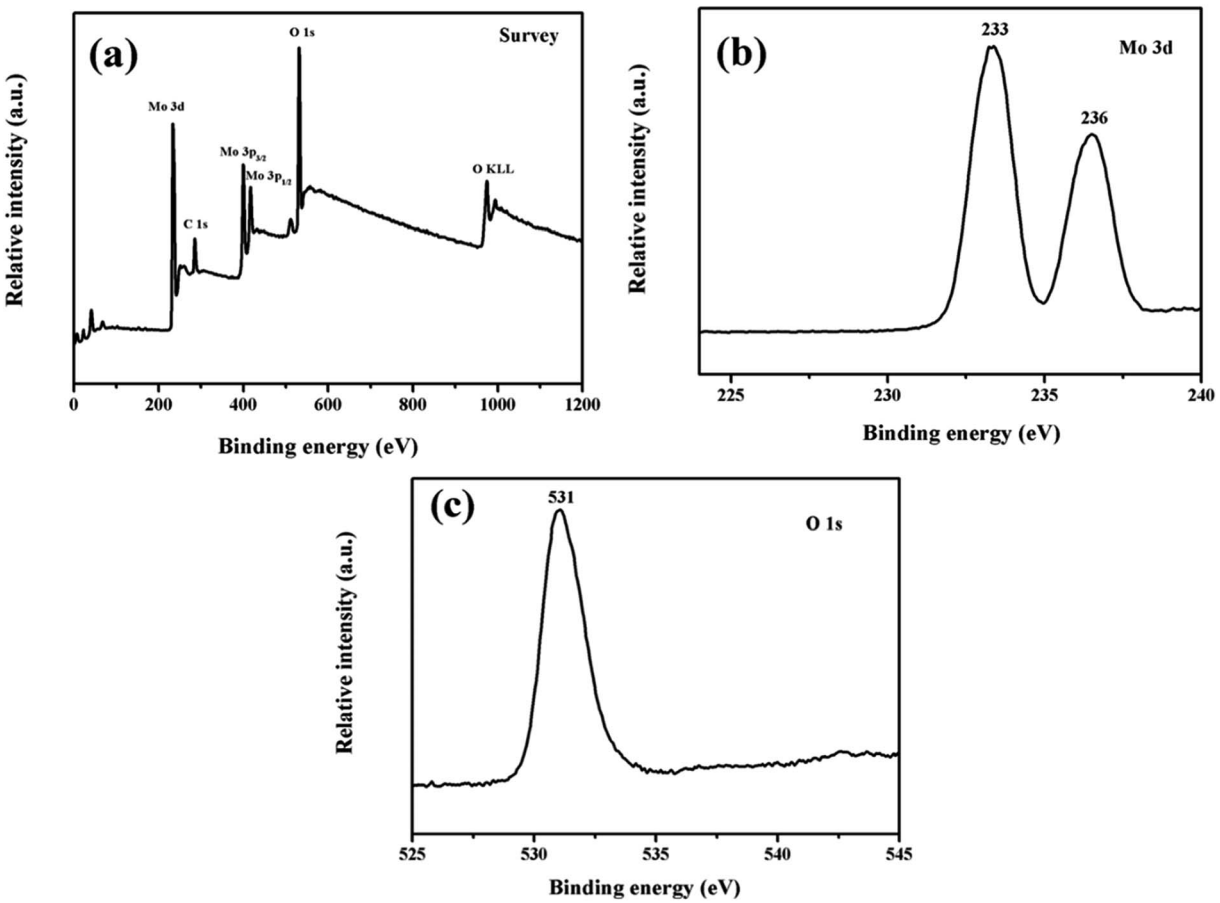


Fig. 3 XPS spectra of the $MoO_3$ (a) a typical survey spectrum (b) Mo 3d core level (c) O 1s core level.

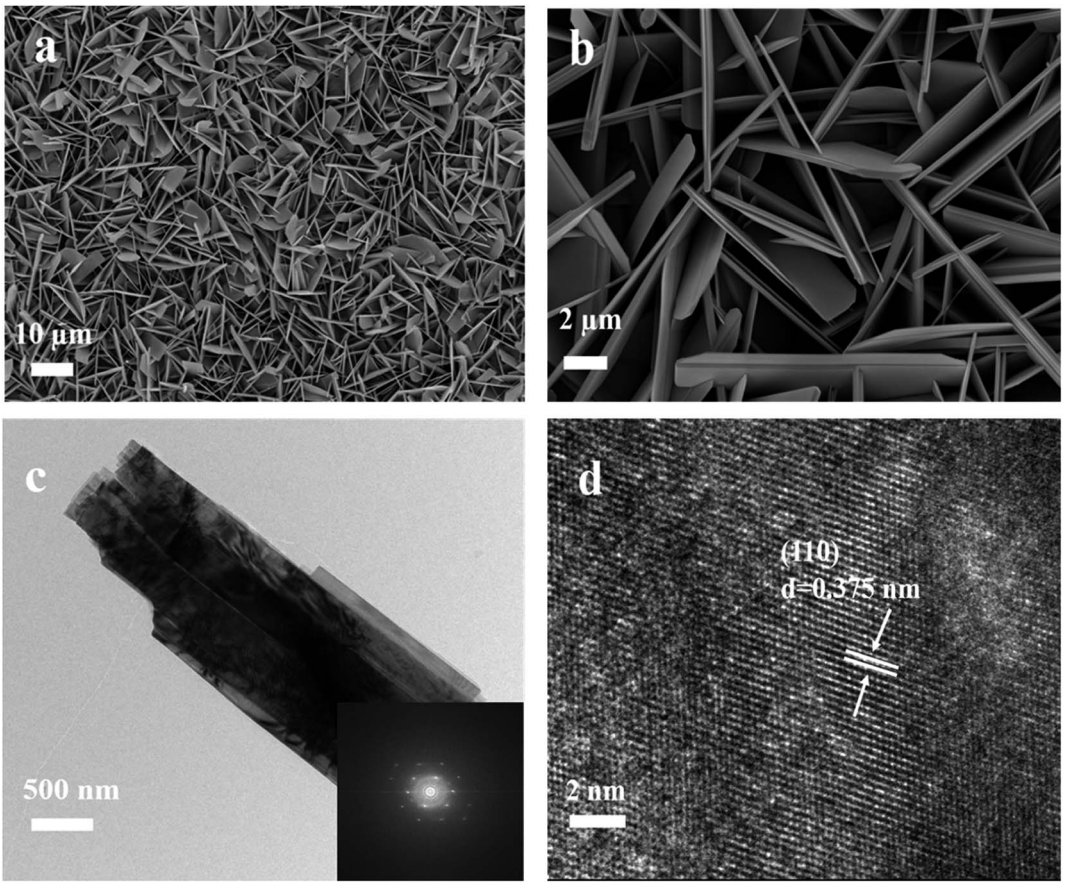


Fig. 4 (a and b) SEM and (c and d) TEM images of $MoO_3$ nanosheets.

which form 3D network structure and possess large surface area. Fig. 4(c) is the TEM image of $MoO_3$ nanosheet and Fig. 4(d) is the HRTEM image. It can be found that the as-prepared $MoO_3$ is well-crystallized and the lattice spacing is 0.375 nm, which belongs to the (110) plane.

To investigate the light absorption properties of the as-prepared $MoO_3$, the UV-Vis absorption spectra of the $MoO_3$ was recorded and displayed in Fig. 5. It can be seen that there is a broad absorbance peak during 200–450 nm, and band gap is estimated to be 2.9 eV from the plots of $(\alpha h\nu)^2$ *versus* photon energy $h\nu$.[37]

### 3.2 Growth mechanism

In this work, the $MoO_3$ nanosheets which grown vertically on the surface of quartz tablet were fabricated *via* CVD method. During the CVD process, $MoS_2$ was steamed up in the high-temperature area. Then it was reacted with oxygen and meanwhile driven by Ar, then deposited gradually on the surface of the quartz tablet in the low-temperature area. Therefore, the growing mechanism of the morphology is based on the vapor-solid (VS) mechanism. According to VS mechanism, the size of the nanosheet is proportional to the time and growth rate, which is depend on the evaporation rate and pressure. According to $P = B\exp\left\{\frac{-\pi\sigma^2}{(kT)^2\ln(\alpha)}\right\}$, $P$ is the probability of nucleation, $B$ is a constant, $\sigma$ is the surface energy of solid whiskers, $k$ is the boltzmann constant, $T$ is the absolute temperature, $\alpha$ is the supersaturation ratio (defined as: $\alpha = p/p_0$, $p$ and $p_0$ are the initial pressure and equilibrium pressure at the corresponding ambient temperature respectively). Evaporation rate and system pressure may increase by affecting the

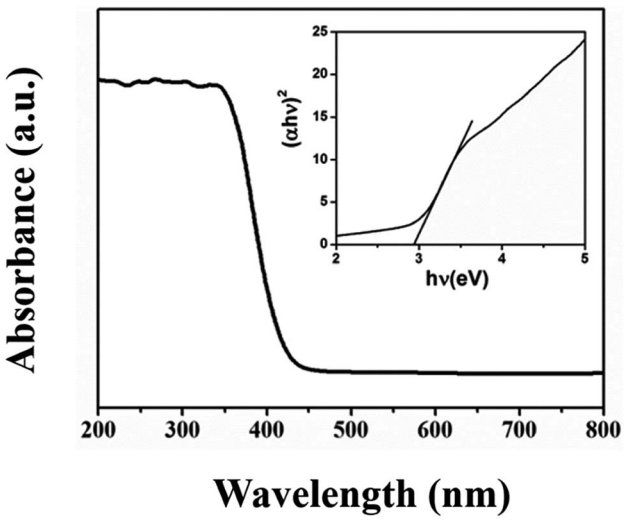


Fig. 5 UV-Vis spectra of $MoO_3$.

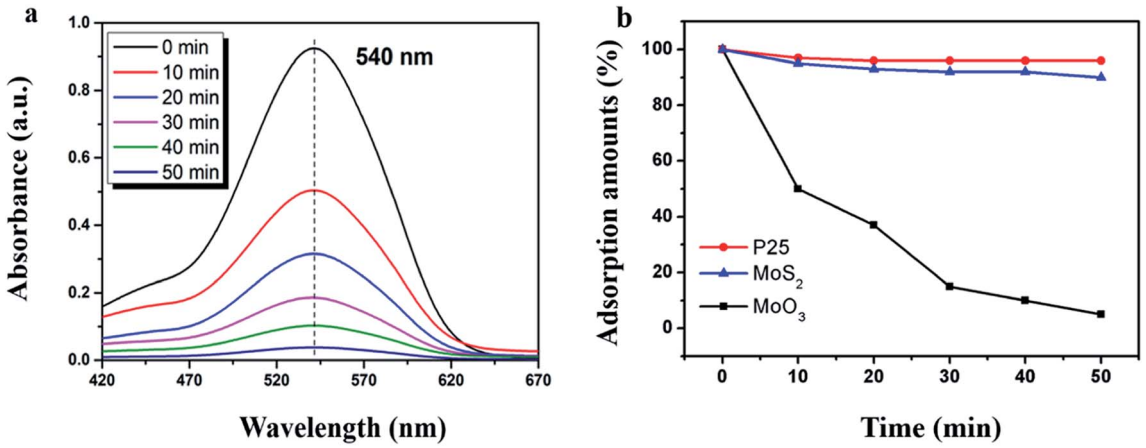


Fig. 6 (a) Photocatalytic efficiency of $MoO_3$ and (b) degradation performance of the referential photocatalysts.

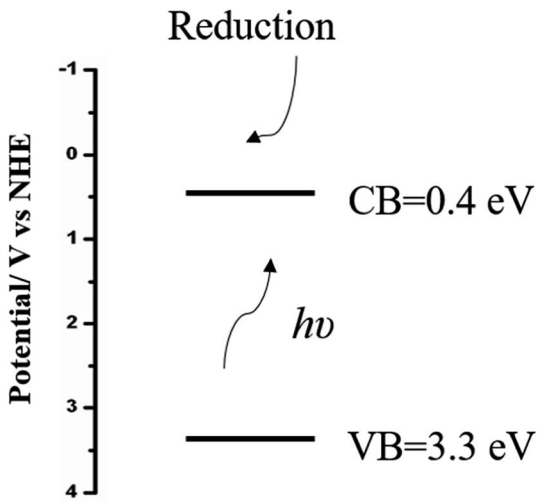


Fig. 7 Photocatalytic mechanism of the as-prepared $MoO_3$ nanosheets.

supersaturated vapor pressure. Thus, $MoO_3$ nanosheets were more easily formed under higher temperature and supersaturation.

### 3.3 Photocatalytic activity of Cr(VI)

Fig. 6(a) displays the photocatalytic efficiency of Cr(VI) under visible light with $MoO_3$ as photocatalyst. It can be found that the intensity of characteristic peak of Cr(VI) gradually weakens as the irradiation time goes on, indicating the degradation of the Cr(VI), which proves that the as-prepared $MoO_3$ can be used to degrade Cr(VI).

P25 and $MoS_2$ nanosheets were used as referential photocatalysts for degradation of Cr(VI), and it can be found that both the P25 and $MoS_2$ nanosheets have little photocatalytic performance on the degradation of Cr(VI) as shown in Fig. 6(b).

The photocatalytic mechanism of the as-prepared $MoO_3$ nanosheets were discussed as shown in Fig. 7. The conduction band and valence band potentials of the semiconductor were

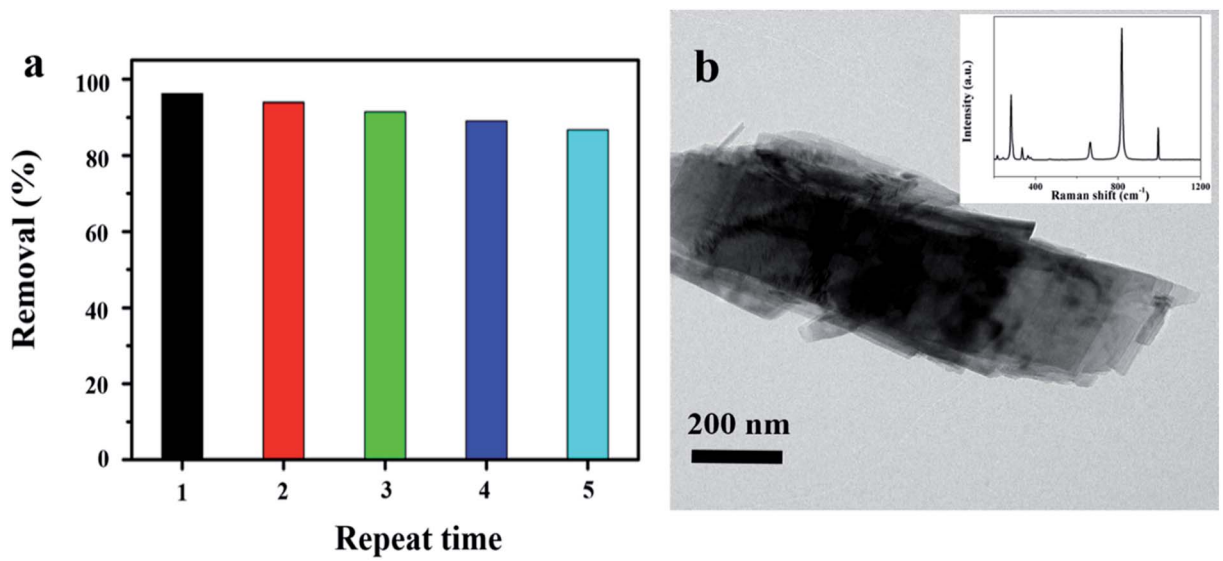


Fig. 8 (a) Recycling of $MoO_3$ for the photocatalytic degradation of Cr(VI) and (b) TEM of $MoO_3$ after reusing. Inset is the Raman spectra.

calculated by $E_{CB} = \varepsilon - E_H - 0.5E_g$ and $E_{VB} = E_{CB} + E_g$. $\varepsilon$ is the absolute electronegativity of an atom semiconductor, which is defined as the arithmetic mean of the atomic electro affinity and the first ionization energy; $E_H$ is the energy of free electrons of hydrogen scale (4.5 eV); $E_{CB}$ and $E_{VB}$ are the potentials of the conduction and valence bands, respectively, while $E_g$ is the band gap between the conduction and valence bands.[28,38] Therefore, the conduction and valence band positions of $MoO_3$ were calculated to be 0.4 eV and 3.3 eV, respectively.

The photo-excited electrons converge on the conduction band of the $MoO_3$ and reduce the absorbed oxygen molecules on the $MoO_3$ surface, inducing a chain of reactions as follows:[34]

$$MoO_3 + h\nu \rightarrow MoO_3 (h^+ + e^-) \quad (1)$$

$$6e^- + Cr_2O_7^{2-} + 14H^+ \rightarrow 2Cr^{3+} + 7H_2O \quad (2)$$

The recycling of $MoO_3$ nanosheets used for photocatalytic degradation of Cr(VI) under visible-light irradiation was investigated and the results can be found in Fig. 8.

The recycling test showed that the photocatalytic activity did not exhibit obvious reduction during the recycling, and the Cr(VI) removal of 85% can still be achieved even after recycling for five times. According to the TEM and Raman analysis, it can be found that there was almost no change of the morphology and structure of $MoO_3$, which meant the recyclable of the as-prepared photocatalyst.

## 4. Conclusions

$MoO_3$ nanosheets were fabricated and deposited vertically on the surface of quartz tablet by one-step CVD method. The $MoO_3$ nanosheets exhibited good photocatalytic efficiency for degradation of Cr(VI). The catalyst was easy to be separated from water and almost retained the catalytic efficiency after reused five times. Thus, the as-prepared $MoO_3$ has a clear advantage for applications in environmental fields.

## Conflicts of interest

There are no conflicts to declare.

## Acknowledgements

This work is funded by New methods of analysis and testing of Jiangsu Association for Instrumental Analysis.

## References

1 J. Ye, J. Liu, Z. Huang, S. Wu, X. Dai, L. Zhang and L. Cui, Effect of reduced graphene oxide doping on photocatalytic reduction of Cr(VI) and photocatalytic oxidation of tetracycline by ZnAlTi layered double oxides under visible light, *Chemosphere*, 2019, **227**, 505–513.
2 Y. Mu, Z. Ai, L. Zhang and F. Song, Insight into Core–Shell Dependent Anoxic Cr(VI) Removal with Fe@$Fe_2O_3$ Nanowires: Indispensable Role of Surface Bound Fe(II), *ACS Appl. Mater. Interfaces*, 2015, **7**, 1997–2005.
3 W. Zhao, J. Li, B. Dai, Z. Cheng, J. Xu, K. Ma, L. Zhang, N. Sheng, G. Mao, H. Wu, K. Wei and D. Y. C. Leung, Simultaneous removal of tetracycline and Cr(VI) by a novel three dimensional AgI/$BiVO_4$ p–n junction photocatalyst and insight into the photocatalytic mechanism, *Chem. Eng. J.*, 2019, **369**, 716–725.
4 T. Sakthivel, G. Venugopal, A. Durairaj, S. Vasanthkumar and X. Huang, Utilization of the internal electric field in semiconductor photocatalysis: a short review, *J. Ind. Eng. Chem.*, 2019, **72**, 18–30.
5 D. Venkatesh, S. Pavalamalar and K. Anbalagan, Selective photodegradation on dual dye system by recoverable Nano $SnO_2$ photocatalyst, *J. Inorg. Organomet. Polym. Mater.*, 2019, **29**, 939–953.
6 T. Xu, S. Wang, L. Li and X. Liu, Dual templated synthesis of tri-modal porous $SrTiO_3/TiO_2$@ carbon composites with enhanced photocatalytic activity, *Appl. Catal., A*, 2019, **575**, 132–141.
7 X. Tao, Y. Gao, S. Wang, X. Wang, Y. Liu, Y. Zhao, F. Fan, M. Dupuis, R. Li and C. Li, Interfacial charge modulation: an efficient strategy for boosting spatial charge separation on semiconductor photocatalysts, *Adv. Energy Mater.*, 2019, 1803951.
8 Z. Liu, J. Tian, D. Zeng, C. Yu, W. Huang, K. Yang, X. Liu and H. Liu, Binary-phase $TiO_2$ modified $Bi_2MoO_6$ crystal for effective removal of antibiotics under visible light illumination, *Mater. Res. Bull.*, 2019, **112**, 336–345.
9 Y. Li, T. Liu, T. Li and X. Peng, Hydrothermal fabrication of controlled morphologies of $MoO_3$ with CTAB: Structure and growth, *Mater. Lett.*, 2015, **140**, 48–50.
10 S. Dhanavel, E. A. K. Nivethaa, K. Dhanapal, V. K. Gupta, V. Narayanan and A. Stephen, a-$MoO_3$/polyaniline composite for effective scavenging of rhodamine B, congo red and textile dye effluent, *RSC Adv.*, 2016, **6**, 28871–28876.
11 L. Khandare and D. J. Late, $MoO_3$-rGO nanocomposites for electrochemical energy storage, *Appl. Surf. Sci.*, 2017, **418**, 2–8.
12 J. Huang, J. Yan, J. Li, L. Cao, Z. Xu, J. Wu, L. Zhou and Y. Luo, Assembled-sheets-like $MoO_3$ anodes with excellent electrochemical performance in Li-ion battery, *J. Alloys Compd.*, 2016, **688**, 588–595.
13 L. Wang, G. Zhang, Y. Sun, X. Zhou and K. Chou, Preparation of ultrafine β-$MoO_3$ from industrial grade $MoO_3$ powder by the method of sublimation, *J. Phys. Chem. C*, 2016, **120**, 19821–19829.
14 R. Pandeeswari and B. G. Jeyaprakash, Nanostructured α-$MoO_3$ thin film as a highly selective TMA sensor, *Biosens. Bioelectron.*, 2014, **53**, 182–186.
15 G. P. Nagabhushana, D. Samrat and G. T. Chandrappa, a-MoO3 nanoparticles: solution combustion synthesis, photocatalytic and electrochemical properties, *RSC Adv.*, 2014, **4**, 56784–56790.
16 C. I. Fernandes, S. C. Capelli, P. D. Vaz and C. D. Nunes, Highly selective and recyclable $MoO_3$ nanoparticles in epoxidation catalysis, *Appl. Catal., A*, 2015, **504**, 344–350.

17 J. Gong, W. Zeng and H. Zhang, Hydrothermal synthesis of controlled morphologies of $MoO_3$ nanobelts and hierarchical structures, *Mater. Lett.*, 2015, **154**, 170–172.

18 L. Su, Y. Xiong, Z. Chen, Z. Duan, Y. Luo, D. Zhu and X. Ma, $MoO_3$ nanosheet-assisted photochemical reduction synthesis of Au nanoparticles for surface-enhanced Raman scattering substrates, *Sens. Actuators, B*, 2019, **279**, 320–326.

19 E. D. B. Santos, F. A. Sigoli and I. O. Mazali, Structural evolution in crystalline $MoO_3$ nanoparticles with tunable size, *J. Solid State Chem.*, 2012, **190**, 80–84.

20 R. Nadimicherla, W. Chen and X. Guo, Synthesis and characterization of a-$MoO_3$ nanobelt composite positive electrode materials for lithium battery application, *Mater. Res. Bull.*, 2015, **66**, 140–146.

21 Q. Liu, J. Hu, Y. Liang, Z. C. Guan, H. Zhang, H. P. Wang and R. G. Du, Preparation of $MoO_3/TiO_2$ composite films and their application in photoelectrochemical anticorrosion, *J. Electrochem. Soc.*, 2016, **163**, C539–C544.

22 S. Wang, Y. Zhang, T. Chen and G. Wang, Preparation and catalytic property of $MoO_3/SiO_2$ for disproportionation of methyl phenyl carbonate to diphenyl carbonate, *J. Mol. Catal. A: Chem.*, 2015, **398**, 248–254.

23 T. Yunusi, C. Yang, W. Cai, F. Xiao, J. Wang and X. Su, Synthesis of $MoO_3$ submicron belts and $MoO_2$ submicron spheres *via* polyethylene glycol-assisted hydrothermal method and their gas sensing properties, *Ceram. Int.*, 2013, **39**, 3435–3439.

24 S. Alizadeh and S. A. Hassanzadeh-Tabrizi, $MoO_3$ fibers and belts: molten salt synthesis, characterization and optical properties, *Ceram. Int.*, 2015, **41**, 10839–10843.

25 D. Yan, X. Luo, H. Zhang, G. Zhu, L. Chen, G. Chen, H. Xu and A. Yu, Single-crystalline a-$MoO_3$ microbelts derived from a bio-templating method for superior lithium storage application, *J. Alloys Compd.*, 2016, **688**, 481–486.

26 A. Chithambararaj, N. S. Sanjini, S. Velmathi and A. C. Bose, Preparation of h-$MoO_3$ and α-$MoO_3$ nanocrystals: comparative study on photocatalytic degradation of methylene blue under visible light irradiation, *Phys. Chem. Chem. Phys.*, 2013, **15**, 14761–14769.

27 L. Huang, W. Fang, Y. Yang, J. Wu, H. Yu, X. Dong, T. Wang, Z. Liu and B. Zhao, Three-dimensional $MoO_3$ nanoflowers assembled with nanosheets for rhodamine B degradation under visible light, *Mater. Res. Bull.*, 2018, **108**, 38–45.

28 Y. Liu, P. Feng, Z. Wang, X. Jiao and F. Akhtar, Novel fabrication and enhanced photocatalytic MB degradation of hierarchical porous monoliths of $MoO_3$ nanoplates, *Sci. Rep.*, 2016, **7**, 1845.

29 R. Karthiga, B. Kavitha, M. Rajarajan and A. S. Registrar, Synthesis of $MoO_3$ microrods *via* phytoconsituents of Azadirachta indica leaf to study the cationic dye degradation and antimicrobial properties, *J. Alloys Compd.*, 2018, **753**, 300–307.

30 C. Ma, J. Zhou, Z. Cui, Y. Wang and Z. Zou, In situ growth $MoO_3$ nanoflake on conjugated polymer: an advanced photocatalyst for hydrogen evolution from water solution under solar light, *Sol. Energy Mater. Sol. Cells*, 2016, **150**, 102–111.

31 J. Zhou, H. Zeng, Y. Wang and Y. Li, $H^+$ intercalation into molybdenum oxide nanosheets under AFM tip bias, *Phys. Status Solidi RRL*, 2018, **12**, 1700439.

32 T. H. Chiang and H. C. Yeh, The Synthesis of α-$MoO_3$ by ethylene glycol, *Materials*, 2013, **6**, 4609–4625.

33 G. Zhou, Y. Shan, Y. Hu, X. Xu, L. Long, J. Zhang, J. Dai, J. Guo, J. Shen, S. Li, L. Liu and X. Wu, Half-metallic carbon nitride nanosheets with microgrid mode resonance structure for efficient photocatalytic hydrogen evolution, *Nat. Commun.*, 2018, **9**, 3366.

34 J. Yu, S. Zhuang, X. Xu, W. Zhu, B. Feng and J. Hu, Photogenerated electron reservoir in hetero-p–n CuO–ZnO nanocomposite device for visible-light driven photocatalytic reduction of aqueous Cr(VI), *J. Mater. Chem. A*, 2015, **3**, 1199–1207.

35 S. Zhuang, X. Xu, B. Feng, J. Hu, Y. Pang, G. Zhou, L. Tong and Y. Zhou, Photogenerated carriers transfer in dye–graphene–$SnO_2$ composites for highly efficient visible-light photocatalysis, *ACS Appl. Mater. Interfaces*, 2014, **6**, 613–621.

36 N. Qureshi, M. Shinde, S. Arbuj, S. Rane, A. Bhalerao, H.-U. Kim, T. Kim and D. Amalnerkar, Sol–Gel assisted isotropic morphological progression in nanostructured $MoO_3$ and allied investigations on photocatalytic dye-degradation, *J. Nanosci. Nanotechnol.*, 2019, **19**, 3479–3486.

37 J. Y. Bae and S. G. Jang, Preparation and Characterization of CuO-$TiO_2$ composite hollow nanospheres with enhanced photocatalytic activity under visible light irradiation, *J. Nanosci. Nanotechnol.*, 2019, **19**, 6363–6368.

38 G. Zhou, X. Xu, J. Yu, B. Feng, Y. Zhang, J. Hu and Y. Zhou, Vertically aligned $MoS_2/MoO_x$ heterojunction nanosheets for enhanced visible-light photocatalytic activity and photostability, *CrystEngComm*, 2014, **38**, 9025–9032.